

NONSTATIONARY ETAS MODELS FOR NONSTANDARD EARTHQUAKES

BY TAKAO KUMAZAWA^{1,*} AND YOSHIKO OGATA^{1,2,*,†}

The Institute of Statistical Mathematics and University of Tokyo†*

The conditional intensity function of a point process is a useful tool for generating probability forecasts of earthquakes. The epidemic-type aftershock sequence (ETAS) model is defined by a conditional intensity function, and the corresponding point process is equivalent to a branching process, assuming that an earthquake generates a cluster of offspring earthquakes (triggered earthquakes or so-called aftershocks). Further, the size of the first-generation cluster depends on the magnitude of the triggering (parent) earthquake. The ETAS model provides a good fit to standard earthquake occurrences. However, there are nonstandard earthquake series that appear under transient stress changes caused by aseismic forces such as volcanic magma or fluid intrusions. These events trigger transient nonstandard earthquake swarms, and they are poorly fitted by the stationary ETAS model. In this study, we examine nonstationary extensions of the ETAS model that cover nonstandard cases. These models allow the parameters to be time-dependent and can be estimated by the empirical Bayes method. The best model is selected among the competing models to provide the inversion solutions of nonstationary changes. To address issues of the uniqueness and robustness of the inversion procedure, this method is demonstrated on an inland swarm activity induced by the 2011 Tohoku-Oki, Japan earthquake of magnitude 9.0.

1. Introduction. The epidemic-type aftershock sequence (ETAS) model [Ogata (1985, 1986, 1988, 1989)] is one of the earliest point-process models created for clustered events. It is defined in terms of a conditional intensity [Hawkes (1971), Hawkes and Adamopoulos (1973), Ogata (1978, 1981)],

Received October 2013; revised April 2014.

¹Supported by JSPS KAKENHI Grant Numbers 23240039 and 26240004, supported by a postdoctoral fellowship from the Institute of Statistical Mathematics.

²Supported by the Aihara Innovative Mathematical Modelling Project, the “Funding Program for World-Leading Innovative R&D on Science and Technology (FIRST Program),” initiated by the Council for Science and Technology Policy.

Key words and phrases. Akaike Bayesian Information Criterion, change point, two-stage ETAS model, time-dependent parameters, induced seismic activity.

<p>This is an electronic reprint of the original article published by the Institute of Mathematical Statistics in <i>The Annals of Applied Statistics</i>, 2014, Vol. 8, No. 3, 1825–1852. This reprint differs from the original in pagination and typographic detail.</p>

is equivalent to epidemic branching processes [Kendall (1949), Hawkes and Oakes (1974)], and allows each earthquake to generate (or trigger) offspring earthquakes. Besides being used in seismology, the ETAS model has been applied to various fields in the social and natural sciences [e.g., Balderama et al. (2012), Chavez-Demoulina and McGillb (2012), Hassan Zadeh and Sharda (2012), Herrera and Schipp (2009), Mohler et al. (2011), Peng, Schoenberg and Woods (2005), Schoenberg, Peng and Woods (2003)].

Similar magnitude-dependent point-process models have been applied to seismological studies [Vere-Jones and Davies (1966), Lomnitz (1974), Kagan and Knopoff (1987)] and statistical studies [Vere-Jones (1970)]. The ETAS model is stationary if the immigration rate (background seismicity rate) of an earthquake remains constant and the branching ratio is subcritical [Hawkes (1971), Hawkes and Oakes (1974), Zhuang and Ogata (2006)].

The history-dependent form of the ETAS model on occurrence times and sizes (magnitudes) lends itself to the accumulated empirical studies by Utsu (1961, 1962, 1969, 1970, 1971, 1972) and Utsu and Seki (1955), and its establishing history is detailed by Utsu, Ogata and Matsu'ura (1995). ETAS model parameters can be estimated from earthquake occurrence data by maximizing the log-likelihood function to provide estimates for predicting seismic activity (i.e., number of earthquakes per unit time). The model has been frequently used and cited in seismological studies, especially to compare the features of simulated seismicity with those of real seismicity data. The model is also recommended for use in short-term predictions [Jordan, Chen and Gasparini (2012)] in the report of the International Commission on Earthquake Forecasting for Civil Protection. It is planned to be adopted for operational forecasts of earthquakes in California (The Uniform California Earthquake Rupture Forecast, Version 3, URL: http://www.wgcep.org/sites/wgcep.org/files/UCERF3_Project_Plan_v55.pdf).

The ETAS model has also been used to detect anomalies such as quiescence in seismicity. Methods and applications are detailed in Ogata (1988, 1989, 1992, 1999, 2005, 2006a, 2007, 2010, 2011a, 2012), Ogata, Jones and Toda (2003), Kumazawa, Ogata and Toda (2010), and Bansal and Ogata (2013). A change-point analysis examines a simple hypothesis that specific parameters change after a certain time. The misfit of occurrence rate prediction after a change point is then preliminarily shown by the deviation of the empirical cumulative counts of the earthquake occurrences from the predicted cumulative function. The predicted function is the extrapolation of the model fitted before the change point. A downward and upward deviation corresponds to relative quiescence and activation, respectively.

This study considers a number of nonstationary extensions of the ETAS model to examine more detailed nonstandard transient features of earthquake series. The extended models take various forms for comparison with the reference ETAS model, which represents the preceding normal activity

in a given focal region. Because changing stresses in the crust are not directly observable, it is necessary to infer relevant quantitative characteristics from seismic activity data. For example, Hainzl and Ogata (2005) and Lombardi, Cocco and Marzocchi (2010) estimated time-dependent background rates (immigration rates) in a moving time window by removing the triggering effect in the ETAS model.

In Section 2, time-dependent parameters for both background rates and productive rates are simultaneously estimated. There, the penalized log-likelihood is considered for the trade-off between a better fit of the non-stationary models and the roughness penalties against overfitting. Then, not only is an optimal strength adjusted for each penalty but also a better penalty function form is selected using the Akaike Bayesian Information Criterion (*ABIC*) [Akaike (1980)]. These parameter constraints together with the existence of a change point are further examined to determine if they improve the model fit. One benefit of this model is that it allows varying parameters to have sharp changes or discontinuous jumps at the change point while sustaining the smoothness constraints in the rest of the period.

In Section 3, the methods are demonstrated by applying the model to a swarm activity. The target activity started after the March 11, 2011 Tohoku-Oki earthquake of magnitude (M) 9.0, induced at a distance from the M9.0 rupture source. Section 4 concludes and discusses the models and methods. The reproducibility of the inversion results is demonstrated in the Appendix by synthesizing the data and re-estimating it using the same procedure.

2. Methods.

2.1. *The ETAS model.* A conditional intensity function characterizes a point (or counting) process $N(t)$ [Daley and Vere-Jones (2003)]. The conditional intensity $\lambda(t|H_t)$ is defined as follows:

$$(1) \quad \Pr\{N(t, t + dt) = 1 | H_t\} = \lambda(t|H_t) dt + o(dt),$$

where H_t represents the history of occurrence times of marked events up to time t . The conditional intensity function is useful for the probability forecasting of earthquakes, which is obtained by integrating over a time interval.

The ETAS model, developed by Ogata (1985, 1986, 1988, 1989), is a special case of the marked Hawkes-type self-exciting process, and has the following specific expression for conditional intensity:

$$(2) \quad \lambda_\theta(t|H_t) = \mu + \sum_{\{i: S < t_i < t\}} \frac{K_0 e^{\alpha(M_i - M_z)}}{(t - t_i + c)^p},$$

where S is the starting time of earthquake observation and M_z represents the smallest magnitude (threshold magnitude) of earthquakes to be treated

in the data set. M_i and t_i represent the magnitude and the occurrence time of the i th earthquake, respectively, and H_t represents the occurrence series of the set (t_i, M_i) before time t . The parameter set θ thus consists of five elements (μ, K_0, c, α, p) . In fact, the second term of equation (2) is a weighted superposition of the Omori–Utsu empirical function [Utsu (1961)] for aftershock decay rates,

$$(3) \quad \lambda_\theta(t) = \frac{K}{(t+c)^p},$$

where t is the elapsed time since the main shock. It is important to note that, while the concept of a main shock and its aftershocks is intuitively classified by seismologists sometime after the largest earthquake occurs, there is no clear discrimination between them in equation (2). That is, each earthquake can trigger aftershocks, and the expected cluster size depends on the magnitude of the triggering earthquake with the parameter α .

The parameter K_0 (earthquakes/day) is sometimes called the “aftershock productivity.” As the name explains, the parameter controls the overall triggering intensity. The factor c (day) is a scaling time to establish the power-law decay rate and allows a finite number of aftershocks at the origin time of a triggering earthquake (a main shock). In practice, the fitted values for c are more likely to be caused by the under-reporting of small earthquakes hidden in the overlapping wave trains of large earthquakes [Utsu, Ogata and Matsu’ura (1995)]. The exponent p is the power-law decay rate of the earthquake rate in equation (3). The magnitude sensitivity parameter α (magnitude⁻¹) accounts for the efficiency of an earthquake of a given magnitude in generating aftershocks. A small α value allows a small earthquake to trigger a larger earthquake more often. Finally, the background (spontaneous) seismicity rate μ represents sustaining external effects and superposed occurrence rates of long-range decays from unobserved past large earthquakes. It also accounts for the triggering effects by external earthquakes.

The FORTRAN program package associated with manuals regarding ETAS analysis is available to calculate the maximum likelihood estimates (MLEs) of θ and to visualize model performances [Ogata (2006b)]. See also http://www.ism.ac.jp/~ogata/Ssg/ssg_softwareE.html.

2.2. *Theoretical cumulative intensity function and time transformation.* Suppose that the parameter values $\theta = (\mu, K, c, \alpha, p)$ of the ETAS, equation (2), are given. The integral of the conditional intensity function,

$$(4) \quad \Lambda_\theta(t|H_t) = \int_S^t \lambda_\theta(u|H_u) du,$$

provides the expected cumulative number of earthquakes in the time interval $[0, t]$. The time transformation from t to τ is based on the cumulative

intensity,

$$(5) \quad \tau = \Lambda(t|H_t),$$

which transforms the original earthquake occurrence time (t_1, t_2, \dots, t_N) into the sequence $(\tau_1, \tau_2, \dots, \tau_N)$ in the time interval $[0, \Lambda(T)]$. If the model represents a good approximation of the real seismicity, it is expected that the integrated function [equation (4)] and the empirical cumulative counts $N(t)$ of the observed earthquakes are similar. This implies that the transformed sequence appears to be a stationary Poisson process (uniformly distributed occurrence times) if the model is sufficiently correct, and appears to be heterogeneous otherwise.

2.3. Two-stage ETAS model and the change-point problem. In change-point analysis, the whole period is divided into two disjointed periods to fit the ETAS models separately, and is therefore called a two-stage ETAS model. This is one of the easiest ways to treat nonstationary data, and is best applied to cases in which parameters are suspected to change at a specific time. Such a change point is observed when a notably large earthquake or slow slip event (regardless of observed or unobserved) occurs in or near a focal region. Many preceding studies [e.g., Ogata, Jones and Toda (2003), Ogata (2005, 2006a, 2007, 2010), Kumazawa, Ogata and Toda (2010)] have adopted this method to their case studies, and details can be found therein.

The question of whether the seismicity changes at some time T_0 in a given period $[S, T]$ is reduced to a problem of model selection. In this analysis, the ETAS models are separately fitted to the divided periods $[S, T_0]$ and $[T_0, T]$, and their total performance is compared to an ETAS model fitted over the whole period $[S, T]$ by the Akaike Information Criterion (*AIC*) [Akaike (1973, 1974, 1977)]. The *AIC* is described as follows:

$$(6) \quad AIC = -2 \max \log L(\theta) + 2k,$$

where $\ln L(\theta)$ represents the log-likelihood of the ETAS model,

$$(7) \quad \log L(\theta) = \sum_{\{i: S < t_i < T\}} \log \lambda_\theta(t_i|H_{t_i}) - \int_S^T \log \lambda_\theta(t|H_t) dt,$$

and k is the number of parameters to be estimated. The variables t_i and H_{t_i} are the same as those in equation (2). Under this criterion, the model with a smaller *AIC* value performs better. It is useful to keep in mind that $\exp\{-\Delta AIC/2\}$ can be interpreted as the relative probability of how a model with a smaller *AIC* value is superior to others [e.g., Akaike (1980)].

Let AIC_0 be the *AIC* of the ETAS model estimated for the whole period $[S, T]$, AIC_1 be that of the first period $[S, T_0]$, and AIC_2 be that of the

second period $[T_0, T]$, therefore,

$$\begin{aligned}
 AIC_0 &= -2 \max_{\theta_0} \log L(\theta_0; S, T) + 2k_0, \\
 (8) \quad AIC_1 &= -2 \max_{\theta_1} \log L(\theta_1; S, T_0) + 2k_1, \\
 AIC_2 &= -2 \max_{\theta_2} \log L(\theta_2; T_0, T) + 2k_2.
 \end{aligned}$$

Let AIC_{12} represent the total AIC from the divided periods, such that

$$(9) \quad AIC_{12} = AIC_1 + AIC_2 + 2q,$$

with q being the degrees of freedom to search for the best change-point candidate T_0 . Next, AIC_{12} is compared against AIC_0 . If AIC_{12} is smaller, the two-stage ETAS model with the change point T_0 fits better than the ETAS model applied to the whole interval. The quantity q monotonically depends on sample size (number of earthquakes in the whole period $[S, T]$) when searching for the maximum likelihood estimate of the change point [Ogata (1992, 1999), Kumazawa, Ogata and Toda (2010), Bansal and Ogata (2013)]. This penalty term q , as well as an increased number of estimated parameters, imposes a hurdle for a change point to be significant, and it is usually rejected when the one-stage ETAS model fits sufficiently well. If the change point T_0 is predetermined from some information other than the data, then $q = 0$. This is often the case when a conspicuously large earthquake occurs within swarm activity, and will be discussed below. Also, even in this case, the overfitting by the change point is avoided by the AIC_{12} of a two-stage ETAS model, which has two times as many parameters of a single stationary ETAS model throughout the whole period.

2.4. Anomaly factor functions for nonstationary ETAS models. Assume that the ETAS model fits the data well for a period of ordinary seismic activity. Then, the concern is whether this model shows a good fit to the seismicity in a forward extended period. If there are misfits, time-dependent compensating factors are introduced to the parameters to be made time-dependent. These factors are termed ‘‘anomaly factor functions’’ and, thus, the transient changes in parameters are tracked. If earthquake activity is very low in and near a target region preceding the transient activity, data from a wider region, such as the polygonal region in Figure 1, is used to obtain a reference stationary ETAS model (Figure 2). Such a model is stable against small local anomalies, and is therefore a good reference model. The reference ETAS model, coupled with the corresponding anomaly factor functions, becomes the nonstationary ETAS model in this study.

Among the parameters of the ETAS model, the background rate μ and the aftershock productivity K_0 are sensitive to nonstationarity. We therefore

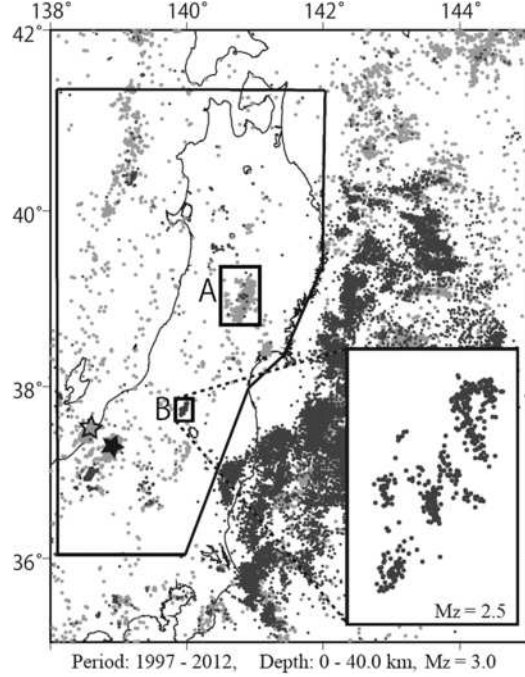


FIG. 1. Epicenters of earthquakes of magnitude (M) ≥ 3.0 in the Northern Honshu region, Japan, with depths shallower than 40 km, from 1997 to 2012, selected from the JMA Hypocenter catalog. The gray and black dots represent the earthquakes that occurred before and after the M9.0 Tohoku-Oki earthquake, respectively. The rectangular regions A and B include the aftershocks of the 2008 Iwate-Miyagi Prefectures Inland Earthquake of M7.2 and the swarm near Lake Inawashiro, respectively. Their inset panels magnify the epicenter distribution with $M \geq 2.0$ and $M \geq 2.5$, respectively. The polygonal region indicates the Tohoku inland and its western offshore region; the earthquakes in this region are used in the reference stationary ETAS model. The closed star represents the epicenter of the 2004 Chuetsu earthquake of M6.8, and the open star represents the 2007 Chuetsu-Oki earthquake of M6.8.

introduce the anomaly factor functions as the nonstationary components to modify the reference stationary ETAS model in such a way that

$$(10) \quad \lambda_{\theta}(t|H_t) = \mu q_{\mu}(t) + \sum_{\{i: S < t_i < t\}} \frac{K_0 q_K(t_i) e^{\alpha(M_i - M_z)}}{(t - t_i + c)^p}.$$

Here $k_{\mu}(t)$ and $q_K(t)$ are referred to as anomaly factor functions of the parameters μ and K_0 , respectively. Because of technical reasons to avoid further model complexity, we did not consider the case in which the other three parameters c , α and p in equation (2) also are time-varying. One structural problem of the ETAS model is that K_0 is correlated with the parameter α . The trade-off is not negligible, especially when the range of

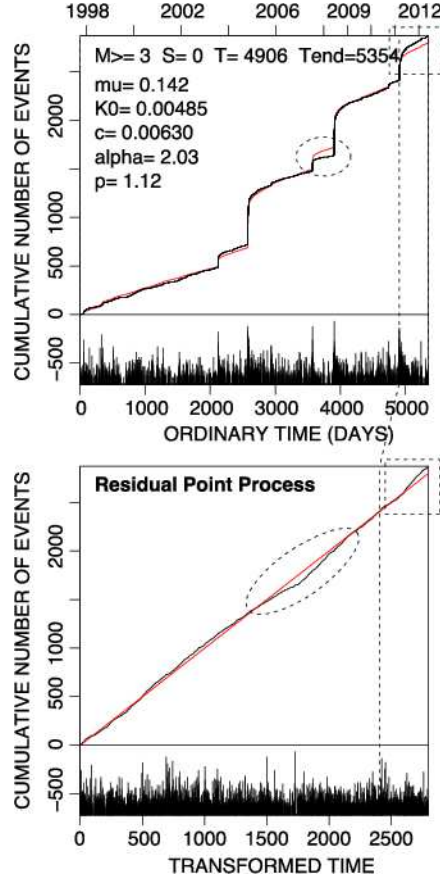


FIG. 2. Cumulative number and magnitude of earthquakes of $M \geq 3$ against the ordinary time and transformed time by the ETAS model from the polygonal region in Figure 1. The fitted period of the model is from October 1997 to the M9.0 March 2011 Tohoku-Oki earthquake (indicated by vertical dashed lines). Red curves in the top and bottom panels represent the theoretical cumulative numbers against the ordinary time (4) and the transformed time, respectively. The dashed black ellipses and dashed rectangles highlight the anomalies around 2008 and after the Tohoku-Oki earthquake, respectively.

magnitudes in the data set is small. See Section 4 for additional discussion of this issue.

We use the first-order spline function of the ordinary time t . This is a broken line interpolated by the coordinates $\{(t_i, q_i); i = 0, 1, 2, \dots, N + 1\}$, where t_i is the occurrence time of the i th earthquake, and t_0 and t_{N+1} are the start and end of the period, respectively. Then, the spline functions are defined as follows:

$$(11) \quad q_\mu(t) = \sum_{i=1}^N I_{(t_i, t_{i+1})}(t) \left\{ \frac{q_{\mu, i+1} - q_{\mu, i}}{t_{i+1} - t_i} (t - t_i) + q_{\mu, i} \right\} = \sum_{i=1}^N q_{\mu, i} F_i(t)$$

and

$$(12) \quad q_K(t) = \sum_{i=1}^N I_{(t_i, t_{i+1})}(t) \left\{ \frac{q_{K,i+1} - q_{K,i}}{t_{i+1} - t_i} (t - t_i) + q_{K,i} \right\} = \sum_{i=1}^N q_{K,i} F_i(t),$$

where $I_{(t_i, t_{i+1})}(t)$ is the indicator function, with the explicit form of $F_i(t)$ given as

$$(13) \quad F_i(t) = \frac{t - t_{i-1}}{t_i - t_{i-1}} I_{(t_{i-1}, t_i)}(t) + \frac{t_{i+1} - t}{t_{i+1} - t_i} I_{(t_i, t_{i+1})}(t).$$

The log-likelihood function of the nonstationary point process can be written as follows:

$$(14) \quad \log L(q) = \sum_{\{i, S < t_i < T\}} \log \lambda_q(t_i | H_{t_i}) - \int_S^T \lambda_q(t | H_t) dt,$$

where $q = (q_\mu, q_K)$.

2.5. *Penalties against rough anomaly factor functions.* Since these anomaly functions have many coefficients representing flexible variations, coefficients are estimated under an imposed smoothness constraint to avoid their overfitting. This study uses the penalized log-likelihood [Good and Gaskins (1971)] described below. With the roughness penalty functions,

$$(15) \quad \begin{aligned} \Phi_\mu &= \sum_{i=0}^N \left(\frac{q_{\mu,i+1} - q_{\mu,i}}{t_{i+1} - t_i} \right)^2 (t_{i+1} - t_i) \quad \text{and} \\ \Phi_K &= \sum_{i=0}^N \left(\frac{q_{K,i+1} - q_{K,i}}{t_{i+1} - t_i} \right)^2 (t_{i+1} - t_i), \end{aligned}$$

and the penalized log-likelihood against the roughness becomes

$$(16) \quad Q(q | w_\mu, w_K) = \log L(q) - w_\mu \Phi_\mu - w_K \Phi_K,$$

where each “ w ” represents weight parameters that tune the smoothness constraints of the anomaly factors. The roughness penalty, equation (15), imposes penalties to the log-likelihood according to parameter differentials at successive event occurrence times.

Furthermore, the degree of the smoothness constraints may not be homogeneous in ordinary time because earthquake series are often highly clustered. In other words, it is expected that more detailed or rapid changes of the anomaly factors appear during dense event periods rather than during sparse periods [Ogata (1989), Adelfio and Ogata (2010)]. Hence, for the same model, alternative constraints are considered by replacing $\{t_i\}$ in equation

TABLE 1

Summary of the competing nonstationary ETAS models. The numbers index the models. The row headers explain the model restrictions of anomaly factors $q_\mu(t)$ and $q_K(t)$. The first column (a) uses smoothing on ordinary time, the second column (b) on the transformed time

Restrictions	(a) Smoothing on ordinary time	(b) Smoothing on transformed time
$q_K(t) = 1$	Model 1(a)	Model 1(b)
$q_\mu(t) = q_K(t)$	Model 2(a)	Model 2(b)
No restriction	Model 3(a)	Model 3(b)

(15) with $\{\tau_i\}$ on the transformed time τ in equation (5) of the reference ETAS model.

The following restricted cases of the nonstationary model in equation (10), together with different types of the aforementioned parameter constraints, are examined and summarized in Table 1. Model 1 restricts the parameter K_0 to be constant and unchanged from the reference model, leaving $q_\mu(t)$ to be unrestricted. Model 2 restricts the parameters μ and K_0 to have the same factor. In other words, model 2 estimates the anomaly factor for the total intensity $\lambda_\theta(t|H_t)$ in equation (10). This restriction is assumed in Adelfio and Ogata (2010). Model 3 has no restriction.

Here, from a statistical modeling viewpoint, it should be noted that μ and K_0 are linearly parameterized regarding the conditional intensity [equation (2)], and likewise the linearly parameterized coefficients of the functions q_μ and q_K in equation (10). Together, they force the penalized log-likelihood function [equation (16)] to be strictly concave regardless of the dimensions of the coefficients' space [Ogata (1978, 2001), Ogata and Katsura (1993)]. Therefore, the maximizing solutions of the penalized log-likelihood function can be obtained uniquely and stably under a suitable numerical optimization algorithm [e.g., appendices of Ogata (2004, 2011b)]. The reproducibility of the inversion results of $\mu(t)$ and $K_0(t)$ are demonstrated in the Appendix.

2.6. Tuning smoothness constraints, model selection and error evaluation.

In a Bayesian context, given the weights, the solution of the parameters q that minimize the penalized log-likelihood Q in (16) is termed the maximum a posteriori (MAP) estimate. In the following section, we describe how to determine the optimal MAP (OMAP) estimate. To obtain the optimal weights in the penalty functions in equation (16), this study uses a Bayesian interpretation of penalized log-likelihood as suggested by Akaike (1980). Specifically, the exponential of each penalty function is proportional to a prior Gaussian distribution of the forms

$$(17) \quad \pi(q_\mu|w_\mu) \propto e^{-w_\mu q_\mu \Sigma_\mu q_\mu^t / 2} \quad \text{and} \quad \pi(q_K|w_K) \propto e^{-w_K q_K \Sigma_K q_K^t / 2},$$

since the coefficients of the function $q(\cdot)$ in the penalty term Φ take a quadratic form with a symmetric $(N+1) \times (N+1)$ nonnegative definite matrix Σ . Since each matrix Σ is degenerate and has $\text{rank}(\Sigma) = N$, above each prior distribution becomes improper [Ogata and Katsura (1993)]. To avoid such improper priors, we divide each of the vectors q into $(q^c, q^{(N+1)})$ so that each of the priors becomes a probability density function with respect to q^c :

$$(18) \quad \pi(q^c|w, q_{N+1}) = \frac{(w^N \det \Sigma^c)^{1/2}}{\sqrt{2\pi}^N} \exp\left(-\frac{1}{2}w^N q^c \Sigma^c q^c\right),$$

where Σ^c is the cofactor of the last diagonal element of Σ , and w and $q^{(N+1)}$ are considered hyperparameters to maximize the integral of the posterior distribution with respect to q^c ,

$$(19) \quad \begin{aligned} & \Psi(w_\mu, w_K; q_\mu^{(N+1)}, q_K^{(N+1)}) \\ &= \int L(q_\mu, q_K) \pi(q_\mu|w_\mu) \pi(q_K|w_K) dq_\mu^c dq_K^c, \end{aligned}$$

which refers to the likelihood of a Bayesian model. Good (1965) suggests the maximization of equation (19) with respect to the hyperparameters and termed this the Type II maximum likelihood procedure.

By applying Laplace's method [Laplace (1774), pages 366–367], the posterior distribution is approximated by a Gaussian distribution, by which the integral in equation (19) becomes

$$(20) \quad \begin{aligned} & \Psi(w_\mu, w_K; q_\mu^{(N+1)}, q_K^{(N+1)}) \\ &= Q(\hat{q}_\mu^c, \hat{q}_K^c | w_\mu, w_K; q_\mu^{(N+1)}, q_K^{(N+1)}) \\ & \quad - \frac{1}{2} \log(\det H_\mu) - \frac{1}{2} \log(\det H_K) + MN \log 2\pi, \end{aligned}$$

where \hat{q} is the maximum of the penalized log-likelihood Q in equation (16) and

$$(21) \quad H(\hat{q}^c | w, q^{(N+1)}) = \frac{\partial^2 \log L(\hat{q}^c | w, q^{(N+1)})}{\partial q^c \partial (q^c)^t} - \Sigma^c(w, q^{(N+1)}),$$

for a fixed weight w for either w_μ or w_K .

Thus, maximizing equation (16) with respect to q^c and equation (20) with respect to $(w_\mu, w_K; q_\mu^{(N+1)}, q_K^{(N+1)})$, in turn, achieves our objective. In the former maximization, a quasi-Newton method using the gradients $\partial \log L(q) / \partial q$ and the Newton method making use of the Hessian matrices, equation (21), endure a fast convergence regardless of high dimensions. For the latter maximization, a direct search such as the simplex method is used. A flowchart of numerical algorithms is described in the appendices of Ogata (2004, 2011b).

Anomaly factor functions under the optimal roughness penalty result in suitably smooth curves throughout the period. Furthermore, there may be a change point that results in sudden changes in parameters μ or K . To examine such a discontinuity, a sufficiently small weight is put into the interval that includes a change point (e.g., $w = 10^{-5}$), and the goodness-of-fit by *ABIC* is compared with that of the smooth model with the optimal weights for all intervals.

It is useful to obtain the estimation error bounds of the MAP estimate \hat{q} at each time of an observed earthquake. The joint error distribution of the parameters at \hat{q} is nearly a $2N$ -dimensional normal distribution $N(0, H^{-1})$, where $H^{-1} = (h^{i,j})$, and $H = (h_{i,j})$ is the Hessian matrix in equation (21). Hence, the covariance function of the error process becomes

$$(22) \quad c(u, v) = \sum_{i=1}^{2N} \sum_{j=1}^{2N} F_i(u) h^{i,j} F_j(v),$$

where $F_i = F_{N+i}$ for $i = 1, 2, \dots, N$, which is defined in equation (13). Thus, the standard error of q is provided by

$$(23) \quad \varepsilon(t) = [\varepsilon_\mu(t), \varepsilon_K(t)] = \sqrt{C(t, t)}.$$

2.7. *Bayesian model comparison.* It is necessary to compare the goodness of fit among the competing models. From equation (20), the *ABIC* [Akaike (1980)] can be obtained as

$$(24) \quad \begin{aligned} ABIC = & (-2) \max_{w_\mu, w_K; q_\mu^{(N+1)}, q_K^{(N+1)}} \log \Psi(w_\mu, w_K; q_\mu^{(N+1)}, q_K^{(N+1)}) \\ & + 2 \times (\#\text{hyperparameter}). \end{aligned}$$

Specifically, models 1 and 2 [1(a) and (b), 2(a) and (b) in Table 1] have four hyperparameters, and model 3 [3(a) and (b)] has eight. A Bayesian model with the smallest *ABIC* value provides the best fit to the data.

Since there are various constraints in the different setups, the resulting *ABIC* values cannot be simply compared because of unknown different constants, mainly due to the approximations in equation (20). Alternatively, the difference of *ABIC* values relative to those corresponding to the reference model are used. In other words, the reduction amount of the *ABIC* value from a very heavily constrained case,

$$(25) \quad \Delta ABIC = ABIC - ABIC_0,$$

where *ABIC* is that of equation (24) and $ABIC_0$ is the *ABIC* value with very heavy fixed weights, which constrain the function to be almost constant. Therefore, the $\Delta ABIC$ approximates the *ABIC* improvement from the flat anomaly functions [$q(t) = 1$ for all t] to the optimal functions.

Likewise in AIC , it is useful to keep in mind that $\exp\{-\Delta AIC/2\}$ can be interpreted as the relative probability of how the model with the smallest AIC value is superior to others [e.g., Akaike (1980)].

3. Applications.

3.1. *The stationary ETAS model versus the two-stage ETAS model.* First, we estimate the stationary ETAS model that has been applied to a series of earthquakes of magnitude (M) 3.0 and larger contained in the polygonal region highlighted in Figure 1, from October 1997 to the M9.0 Tohoku-Oki earthquake on March 11, 2011. Specifically, the MLE has been obtained for the stationary ETAS model [equation (2)] by applying a normal activity for earthquakes of M3.0 and larger from October 1997 to March 10, 2011 (Figure 2). According to the estimated theoretical cumulative curve in ordinary time [equation (4)] and transformed time [equation(5)] in Figure 2, the ETAS model appears to fit very well except for a period near 2008 and a period after the Tohoku-Oki earthquake, which is in good accordance with Ogata (2012). These anomalies are highlighted by dashed ellipses and dashed rectangles in Figure 2.

The former is the apparent lowering due to substantially small productivity in the aftershock activity of the 2007 Chuetsu-Oki earthquake (open star in Figure 1). Interestingly enough, the 2004 Chuetsu earthquake (closed star) and the 2007 Chuetsu-Oki earthquake, which are about 40 km apart, have the same magnitude (M6.8), but the number of aftershocks of $M \geq 4.0$ differs by 6–7 times [Japan Meteorological Agency (2009)].

The latter is due to the activation relative to the predicted ETAS model. The March 11, 2011 M9.0 Tohoku-Oki earthquake induces this activation. On the other hand, a series of aftershocks (located in region A, Figure 1) of the 2008 M7.2 Iwate-Miyagi Prefecture inland earthquake is quiet relative to the occurrence rate predicted by the ETAS model estimated from the aftershock data before the M9.0 earthquake.

An analysis of the 2008 earthquake aftershock sequence is shown in Figure 3. Here the ETAS model is fitted to the period from one day after the main shock until the M9.0 earthquake. The estimated intensity is then extrapolated to span an additional year. The change point at the M9.0 earthquake is substantial, decreasing the total AIC by 28.5, showing a relative quiescence afterward. The penalty quantity q in the AIC_{12} of equation (9) equals zero because the change point is given by the information outside of the aftershock data, hence, $\Delta AIC = -28.5$. Therefore, the occurrence of the Tohoku-Oki earthquake is a significant change point.

Hereafter, the data set becomes very difficult for conventional ETAS analysis. The earthquake swarm near Lake Inawashiro began March 18, 2011, a week after the M9.0 earthquake in region B (Figure 1). Seismic activity in

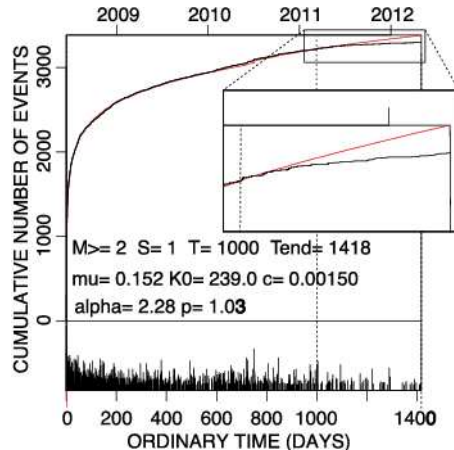


FIG. 3. Cumulative number and magnitude of the aftershock sequence with $M \geq 1.5$, following the 2008 Iwate-Miyagi earthquake of $M7.2$, from the region A against ordinary time. The ETAS model is fitted to the sequence for the period from one day after the main shock ($S = 1.0$ day) to the Tohoku-Oki earthquake (March 11, 2011; dashed line). The almost overlapping red curve indicates the theoretical ETAS cumulative function, equation (4), and the extension to the rest of the period until April 2012. The inset rectangle magnifies the cumulative curve for the extrapolated period.

this area was very low before the $M9.0$ event. The swarm mostly consisted of small earthquakes with magnitudes less than 3.0. The largest earthquake in this cluster, an earthquake of $M4.6$, occurred 50 days after the $M9.0$ earthquake, and its aftershock sequence seemed to decay normally.

First, the stationary ETAS model is applied to the whole period. The theoretical cumulative function (solid light blue curves, Figure 4) is biased below from the empirical cumulative function, indicating a substantial misfit. Hence, the two-stage ETAS model is applied to the data to search the MLE for a change point. Table 2 lists the estimated parameters and AIC values. The change-point analysis (cf. Section 2.2) implies that the MLE of the change point is at $t = 49.8$ days from the beginning of this cluster, which coincides with the time just before the $M4.6$ earthquake occurred. The two-stage ETAS model with this change point improves the AIC by 138.2 (see Table 2). The first-stage ETAS model before the change point, with a fixed parameter $p = 1.0$, still displays a large deviation from the ideal fit (cf. the solid green curve in Figure 4). The magnitude sensitivity parameter α becomes very small relative to that of the second-stage ETAS model. Such a small value implies that almost all earthquakes in the first stage occurred independently to preceding magnitudes (i.e., close to a Poisson process), and can be mostly attributed to the average μ rate of the background seismicity. The first stage μ rate is two orders of magnitude higher than the second stage rate.

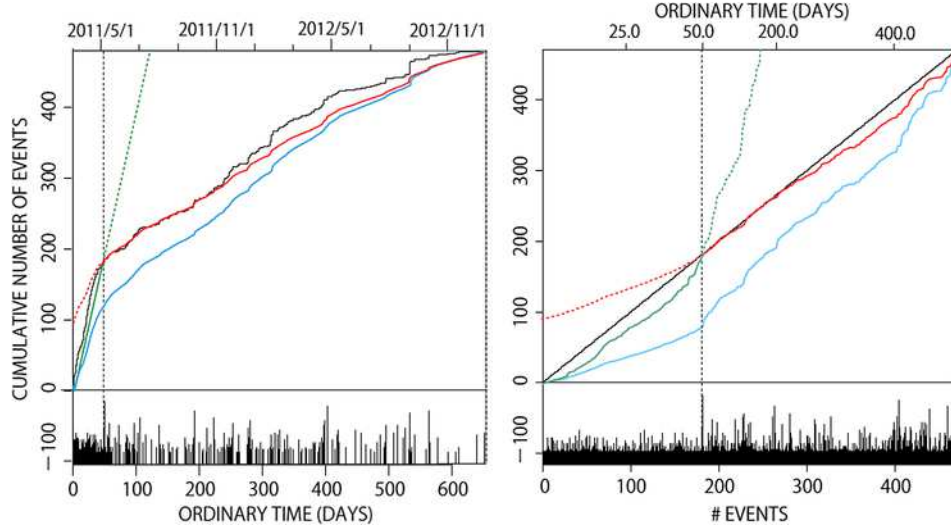


FIG. 4. Stationary and two-stage ETAS models fitted to region B. The ETAS model is fitted to the entire period from March 18, 2011, to the end of 2012 with the preliminary period of the first 0.1 days (blue line), the period before the M4.6 event ($t = 49.8$ days) (green solid line) then extrapolated forward (green dashed line), and the period after the M4.6 event (red solid line) then extrapolated backward (red dashed line). The black curve shows the cumulative number of observed earthquakes. The left panel plots these against ordinary time, whereas the right panel plots these against the number of earthquakes.

TABLE 2

The ETAS parameters of region B fitted to (a) the entire period, (b) and (c) before the change point, and (d) after the change point. Their standard errors are in parentheses. The improvement of the two-stage ETAS model relative to the stationary ETAS model is $\Delta AIC = (422.9 - 118.3) - 442.8 = -138.2$. The MLE for the change point is $t = 49.8$, which coincides with the time just before the M4.6. The threshold magnitude is $M_z = 2.5$. Numbers are rounded to three significant digits

Period	μ	K_0	c	α	p	AIC
(a) The whole period	9.77×10^{-2} (7.81×10^{-2})	6.54×10^{-2} (2.37×10^{-2})	9.64×10^{-4} (6.35×10^{-4})	0.215 (9.77×10^{-2})	0.900 (9.84×10^{-3})	442.8
(b) Before change point with fixed $p = 1.0$	1.41 (3.39×10^{-1})	1.05×10^{-1} (6.99×10^{-2})	8.52×10^{-2} (1.09×10^{-1})	3.06×10^{-15} (9.35×10^{-1})	1.00	-103.0
(c) Before change point without fixed p	1.27 (5.52×10^{-1})	$2.12 \times 10^{+11}$ (4.71)	$1.04 \times 10^{+1}$ (3.81×10^{-1})	2.25×10^{-12} (1.03)	$1.13 \times 10^{+1}$ (2.31×10^{-1})	-118.3
(d) After change point	6.58×10^{-2} (1.43×10^{-1})	3.58×10^{-2} (1.90×10^{-2})	7.11×10^{-5} (1.01×10^{-3})	0.912 (1.10×10^{-1})	0.945 (1.87×10^{-1})	422.9

If p is not fixed, the estimated K_0 , c and p have extremely large values for a normal earthquake sequence while α approaches zero. Consequently, the model is again approximate to a nonstationary Poisson process, characterizing the sequence as a swarm, with an AIC smaller than that of the $p = 1.0$ scenario. The large discrepancies between the estimated parameter values between (b) and (c) in Table 2 suggest that the stationary ETAS model is not well defined for this particular earthquake sequence in the first period before the change point. The standard errors for the parameter α are multiple orders of magnitude greater than those of the estimates themselves. The narrow magnitude range makes it difficult for the model to distinguish the effects of K_0 and α , causing a trade-off between these two parameters, thus providing inaccurate estimations. For the case without a fixed p , the aftershock productivity K_0 becomes extremely small in compensation for the small α estimate.

After the change-point time of the M4.6 earthquake, the ETAS model fits considerably well for several months. Then, a deviation becomes noticeable relative to the solid red cumulative curve in Figure 4. From these observations, it is concluded that the M4.6 earthquake has reduced swarm activity and that decaying normal aftershock type activity has dominated.

3.2. Comparison of the nonstationary models. In this section the proposed nonstationary models and methods outlined in Sections 2.4–2.6 are applied to the same data from region B near Lake Inawashiro. To replicate the transient nonstationary activities in this particular region, we use the seismic activity in the larger polygonal region in Figure 1 for the period before the M9.0 earthquake (MLEs are shown in Figure 2). Such a reference model represents a typical seismicity pattern over a wide region throughout the period, and therefore represents a robust estimate against the inclusion of local and transient anomalies.

By fixing the reference parameters c , α and p , both in the stationary and two-stage ETAS models, μ and K_0 are estimated for events from region B after the M9.0 event, with a magnitude $M \geq 2.5$. Table 3 summarizes the re-estimated parameters, together with the corresponding AIC values. The AIC improvement of the two-stage ETAS model is 126.2.

Next, we have applied the nonstationary ETAS models listed in Table 1, with and without a change point taken into consideration, using the reference parameters in the first row of Table 3. Here, if a change point of M4.6 at the time $t = 49.8$ days occurs, we propose a very small fixed value such as that described in Section 2.5.

Figure 5 shows all of the inversion results (maximum posterior estimates) for a total of 12 models. The $\Delta ABIC$ values of the corresponding models are given in Table 4. Models with the change point outperform corresponding models without the change point. This highlights the significance of jumps

TABLE 3

Reference parameters adjusted to the data from region B and the parameters of the present two-stage ETAS model (standard errors in parentheses) with fixed c , α and p of the reference model (standard errors in brackets), with their AIC values. The improvement of the two-stage ETAS model relative to the present stationary ETAS model is $\Delta AIC = 434.7 - 95.4 - 465.5 = -126.2$. Also, the improvement of the present two-stage ETAS model relative to the stationary ETAS model in Table 2 is as follows: $\Delta AIC = 434.7 - 95.4 - 442.8 = -103.5$. The change point is at $t = 49.8$, corresponding to the time just before the M4.6 earthquake. The threshold magnitude $M_z = 2.5$. Numbers are rounded to three significant digits

Period	μ	K_0	c	α	p	AIC
(a) The whole period	1.92×10^{-1} (3.58×10^{-2})	2.49×10^{-2} (5.82×10^{-3})	6.02×10^{-3} [2.50×10^{-3}]	2.03 [1.27×10^{-2}]	1.11 [5.44×10^{-3}]	465.5
(b) Before the change point	3.31 (1.04×10^{-1})	6.77×10^{-3} (3.27×10^{-3})	602×10^{-3}	2.03	1.11	-95.4
(c) After the change point	1.95×10^{-1} (2.99×10^{-2})	1.56×10^{-2} (6.41×10^{-3})	6.02×10^{-3}	2.03	1.11	434.7

at the change point. Such improvements via jumps are smaller between corresponding models with constraints on the transformed time. This is because those models already present jumps or sharp changes to some extent in the target parameters even without setting change points, due to the expanded transformed time during the dense event period after the M4.6 event in ordinary time. Results also show that models with constraints on ordinary time yield better results than those with the transformed time. This is probably because the data set only contains gradually changing parameters except at the change point.

The smallest $\Delta ABIC$ is achieved by model 3(a') in which both $q_\mu(t)$ and $q_K(t)$ are nonstationary on the smoothness constraints under ordinary time, with a jump at the time of the M4.6 earthquake. Figure 6 shows variations of the background and productivity rates in the selected nonstationary model. These variations suggest that the intensity of aftershock productivity $K_0(t)(=K_0q_K(t))$ is extremely low during early periods of earthquake swarms until the M4.6 earthquake occurs; meanwhile, the background seismicity $\mu(t)(=\mu q_\mu(t))$ changes at a high rate. Therefore, the total seismicity $\lambda_\theta(t|H_t)$ in that period is similar to a nonstationary Poisson process with intensity rates $\mu(t)$ of the background activity. After the M4.6 earthquake occurred, the $\mu(t)$ rate gradually decreased while $K_0(t)$ increased. These changes are roughly approximated by the estimated two-stage ETAS model in Table 3, in which μ before the change point is higher, while K_0 is lower than those after the change point.

If the $\Delta ABIC$ of model 3(a') in Table 4 and ΔAIC of the two-stage ETAS models in Tables 2 and 3 are compared [Akaike (1985, 1987)], the

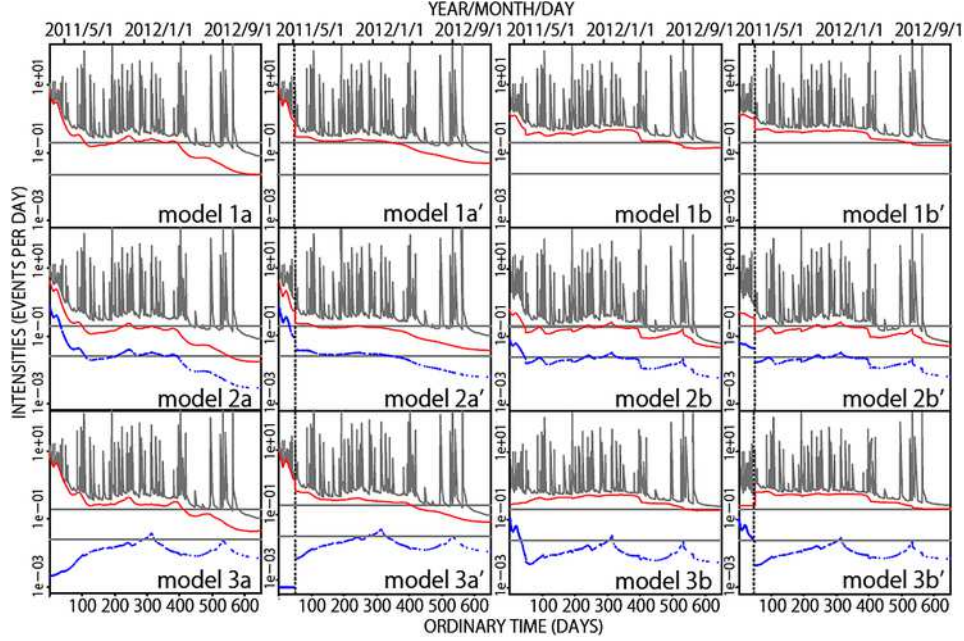


FIG. 5. Various inversion results of all considered models for the data from region B. The model numbers correspond to those of Table 1, and the models with prime (') correspond to those that include a change point. The background rates $\mu(t)$ are shown in red connected lines, and the productivity $K_0(t)$ is shown in blue dots at earthquake occurrence times. The gray spiky curves represent the conditional intensity rates $\lambda(t|H_t)$. The above three functions are plotted on a logarithmic scale. The upper and lower gray horizontal lines represent the reference parameters μ and K_0 , respectively (see Table 2). The vertical dashed line shows the change-point time, $t = 4$ days elapsed from March 18, 2011. The horizontal axis indicates days elapsed.

former model displays a much better fit, with a difference of more than 130. This indicates that the specific details of transient variations in model 3(a') appear to be substantial. Model 3(a') further shows that the background $\mu(t)$ rate decreased after about $t = 400$ days, indicating that the swarm

TABLE 4

$\Delta ABIC$ value of each model defined in equation (25). The underlined model has the smallest value. The prime (') indicates the models that further assume a change point at $t = 49.8$, the time when the $M4.6$ earthquake occurred

Models	a	a'	b	b'
1	-170.0	-177.2	-132.4	-134.1
2	-175.3	-180.1	-136.1	-137.2
3	-250.1	<u>-260.8</u>	-148.1	-151.5

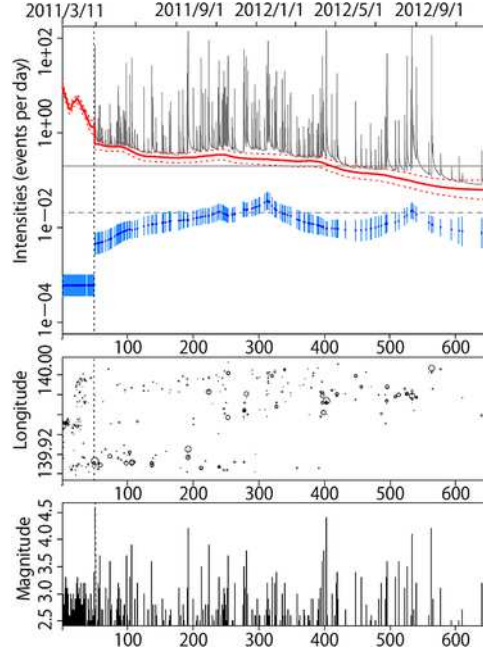


FIG. 6. The selected best-fitted model $3(a')$ and errors of the inversion solutions. The background rate $\mu(t)$ is shown in solid red, with one $-\sigma$ error bounds in red dashed lines. $K_0(t)$ is shown in blue dots with one $-\sigma$ error bars at the occurrence times. The gray spiky curve represents the variation of the intensity rates $\lambda(t|H_t)$. All of the above estimates are plotted on a logarithmic scale. The solid gray horizontal line represents the reference μ value, and the horizontal dashed line represents the reference K_0 value (see Table 2). The horizontal axis is the elapsed days from March 18, 2011. The vertical dashed line shows the change point $t = 49.8$ elapsed days. The middle panel displays the longitudes versus the elapsed times of the earthquake occurrences in region B. The diameters of the circles are proportional to the earthquake magnitudes. The bottom panel shows magnitudes of earthquakes versus the ordinary elapsed times in days.

component of the seismicity decreased. To demonstrate the reproducibility of the detailed variations with the similar data sets, Figure 7 shows the re-estimated model $3(a')$ utilizing the same optimization procedure from simulated data in the estimated model $3(a')$ in Figure 6. See the Appendix for more details.

The model's performance is graphically examined by plotting the estimated cumulative number of events (4) to compare with the observed events in Figure 8, which shows that the observed events become almost a stationary Poisson process, although a few clustering features remain.

It is worthwhile to discuss why model $3(b')$ with constraints under the transformed time has a poorer fit than model $3(a')$ with constraints under ordinary time. The MAP estimate of model $3(b')$ is shown in Figure 9,

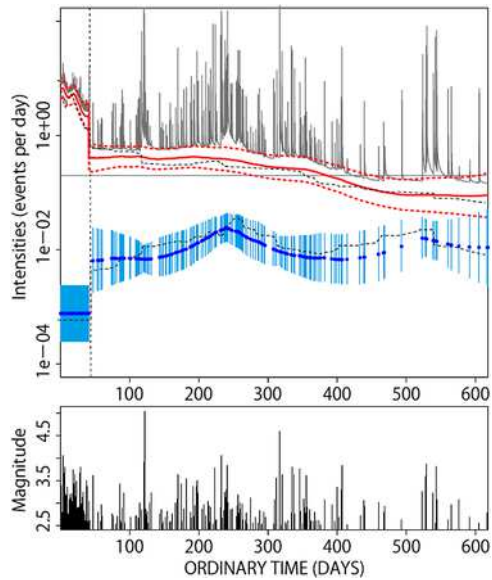


FIG. 7. The maximum a posteriori (MAP) solution of a synthesized data set by the estimated model 3(a') (shown in Figure 6) with the same reference parameters in Table 2. The re-estimated parameters $\mu(t)$ and $K_0(t)$ are shown in red and blue curves, respectively, with two-fold error bounds. The upper and lower dashed black curves represent the true $\mu(t)$ and $K_0(t)$ (same as those in Figure 6), respectively.

where the transformed time τ in this case is defined in equations (4) and (5) using the reference ETAS model, the parameter value of which is listed in the first row of Table 3. Parameter variations in the period after the change point are similar to those of the overall best model 3(a'). Variations during the period before the change point are different with higher $K_0(t)$ and lower $\mu(t)$. However, in this particular application, the performance of model 3(b') on the whole is inferior in terms of $\Delta ABIC$ by a difference of greater than 100. This may be because the above mentioned reference ETAS-based transformed time of the former period worked poorly, unlike during the latter period.

Although the goodness of fit of model 3(b') over the whole period (particularly during the former period) is not quite satisfactory, it is worthwhile to examine the changes of $\mu(\tau)$ and $K_0(\tau)$ during the latter period in Figure 9. The conditional intensity rate $\lambda_\theta(t|H_t)$, background rate $\mu(\tau)$ and aftershock productivity rate $K_0(\tau)$ rapidly decrease not only after the M4.6 earthquake but also after relatively large earthquakes. On such sharp drops, there is a technical but simple explanation. Models in Table 4 with smoothness constraints on the transformed time are sensitive to catalog incompleteness during small time intervals after large earthquakes. In other words, a substantial number of small earthquakes that occur immediately after a large earthquake

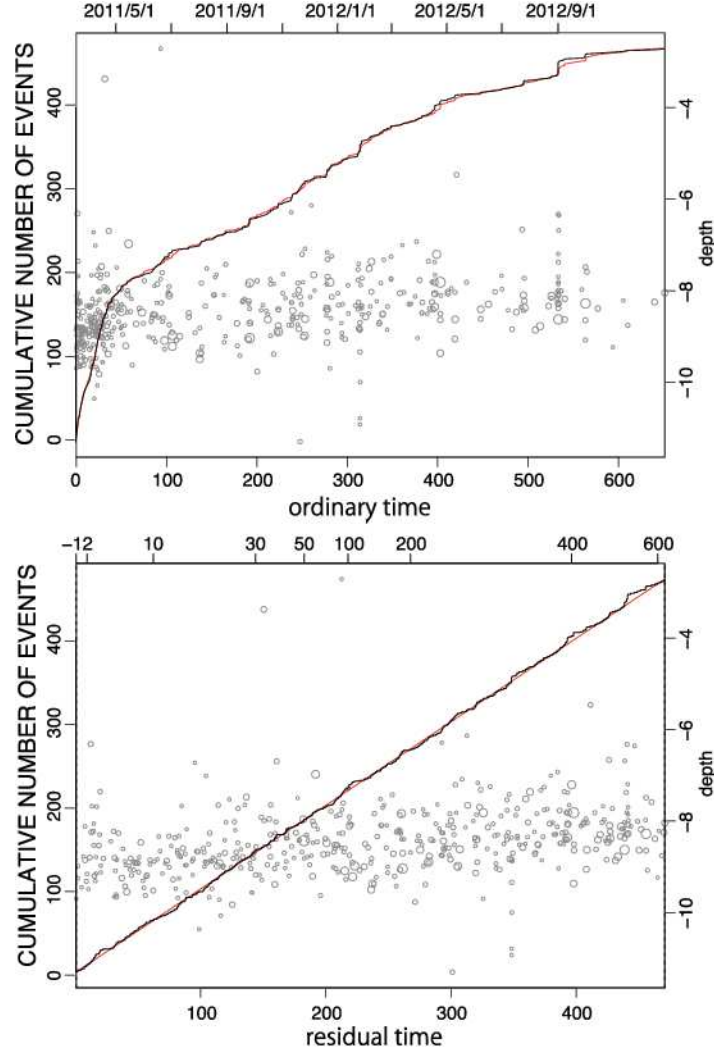


FIG. 8. *Estimated cumulative number of events by model 3(a') (red curves) and the observed number of events (black curve) for the ordinary time (top panel) and residual time (bottom panel). Gray circles show the depths of the swarm events versus the corresponding time.*

are missing in the earthquake catalog [e.g., Ogata and Katsura (2006); Omi et al. (2013)]. Present results suggest that the smoothing on the transformed time can be used as a supplemental tool to check catalog completeness. The time transformation stretches out ordinary time where the intensity rate is high and, hence, transforming the smoothed parameters back to ordinary time can result in sharp changes. This type of constraint can be useful for different applications in which occasional rapid changes are expected.

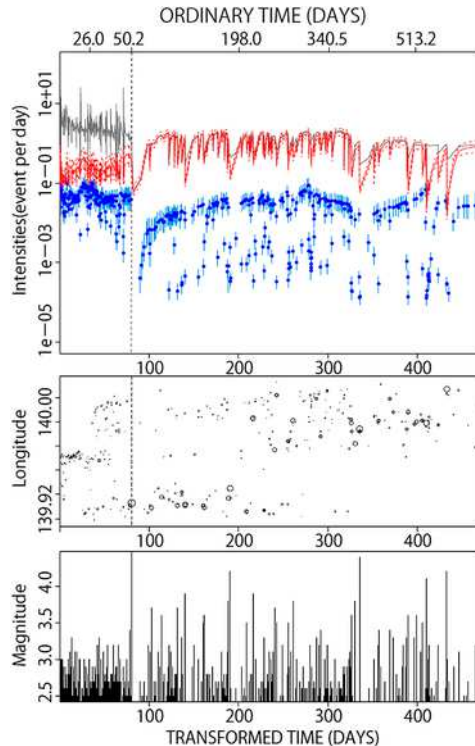


FIG. 9. Variations of conditional intensity rates $\lambda(\tau|H_\tau)$, background rate $\mu(\tau)$ and aftershock productivity $K_0(\tau)$ of model 3(b') versus the transformed time τ of the reference ETAS model (the first row of Table 3). The other details are the same as those in Figure 6.

3.3. *Seismological complements and implications of the results.* Used as a reference model, the polygonal region in Figure 1 is known to have a similar seismicity pattern with similar focal mechanisms under the west–east compressional tectonic field, as described in Terakawa and Matsu’ura (2010) and Toda, Lian and Ross (2011, 2011). For example, earthquakes have mostly north–south strike angles and west–east directional thrust faults in this region. This pattern can also be seen in the configurations of active fault systems on the surface.

In the above sections, the estimation procedures of the models presented here have been illustrated with a data set that includes a cluster of swarm earthquakes triggered by the March 11, 2011 M9.0 Tohoku-Oki earthquake. Swarm activity in this region seems to be triggered by surface waves emitted from the M9.0 source, and has been studied by Terakawa, Hashimoto and Matsu’ura (2013) using the seismological theory and methods used in Terakawa, Miller and Deichmann (2012). Here they attribute swarm activity to the weakening of the fault via an increase of pore fluid pressure caused

by the dynamic triggering effect due to surface waves of the Tohoku-Oki rapture. Thus, the initially very high and then decreasing rate of $\mu(t)$ reflects changes in fault strength, probably due to the intrusion and decrease in pore fluid pressure. The analyses presented here support the quantitative, phenomenological evidence of fault weakening via the intrusion of water into the fault system in earlier periods [Terakawa, Miller and Deichmann (2012, 2013)]. Similarly, by monitoring swarm activity, this nonstationary model can be expected to make quantitative inferences of magma intrusions and draining during volcanic activity.

The background seismicity parameter in the ETAS model is sensitive to transient aseismic phenomena such as slow slips (quiet earthquakes) on and around tectonic plate boundaries [Llenos, McGuire and Ogata (2009), Okutani and Ide (2011)]. This could possibly link a given swarm activity to the weakening of interfaces. Changes in the pore fluid pressure, for example, alter the friction rate of fault interfaces, thereby changing the fault strength. Hence, monitoring the changes in background seismicity has the potential to detect such aseismic events.

Changes in the aftershock productivity K_0 , on the other hand, appear to depend on the locations of earthquake clusters and appear to vary among clusters where secondary aftershocks are conspicuous. The aftershock productivity K_0 therefore reflects the geology around faults rather than the changes in stress rate. The application of the space-time ETAS model with location-dependent parameters [e.g., Ogata, Katsura and Tanemura (2003), Ogata (2004, 2011b)] reveals that the K_0 function varies (i.e., location sensitive) unlike other parameters. Still, the task remains to confirm the link between the changes in ETAS parameters and physical processes happening on and around faults.

4. Conclusions and discussion. There are many examples in seismology in which different authors have obtained differing inversion results for the same scientific phenomenon. These differences are attributed to the adoption of different priors for the parameters of a given model. Scenarios in this study have the same problem and are highlighted in Figure 5. Model parameters in this study are estimated by maximizing the penalized log likelihood, which is intrinsically nonlinear. Besides adjusting the weights in the penalty (namely, hyperparameters of a prior distribution), it is necessary to compare the adequacy of different penalties (prior distributions) associated with the same likelihood function. For these purposes, we have proposed the objective procedure using $\Delta ABIC$ and ΔAIC .

A suitable ETAS model [equation (2)] is first established with MLE as the reference predictive model to monitor future seismic activity and to detect anomalous seismic activity. Sometimes, transient activity starts in a

region with very low seismicity. In such a case, it is both practical and applicable to use a data set from a wider region to estimate the stable and robust parameter values of c , α and p in the ETAS model [equation (2)]. Then, the competing nonstationary ETAS models in equation (10) are fitted together with constraint functions in equations (11) and (12) using either ordinary time or transformed time to penalize the time-dependent parameters in the models. The corresponding Bayesian models include a different prior distribution of the anomaly factor coefficients $q_\mu(\cdot)$ and $q_K(\cdot)$, which are functions of either the ordinary time t [models 1(a)–3(a) in Table 1] or the transformed time τ in the reference ETAS model [models 1(b)–3(b)]. Furthermore, models in which the anomaly functions involve a discontinuity [models 1(a′)–3(a′) and 1(b′)–3(b′)] are considered. Using the $\Delta ABIC$ value, the goodness-of-fit performances of all of the different models are summarized in Table 4. Among the competing models, model 3(a′) attained the smallest $\Delta ABIC$ value, and it is therefore concluded that this model provides the best inversion result for this particular data set.

Thus, changes in background seismicity μ and/or aftershock productivity K_0 of the ETAS model can be monitored. The background seismicity rate in the ETAS models represents a portion of the occurrence rate due to external effects that are not included in the observed earthquake occurrence history in the focal region of interest. Therefore, changes in the background rate have been attracting the interest of many researchers because such changes are sometimes precursors to large earthquakes. The declustering algorithms [e.g., Reasenberg (1985), Zhuang, Ogata and Vere-Jones (2002, 2004)] have been adopted to determine the background seismicity by stochastically removing the clustering components depending on the ratio of the background rate to the whole intensity at each occurrence time. The change-point analysis and nonstationary models presented in this study, however, objectively serve a more quantitatively explicit way to approach this task.

The case where the other three parameters c , α and p in equation (2) also vary with time was not examined in this study. For example, in Figure 8, we have seen that the best model in our framework does not capture all of the clustering events but misses a few small clusters, which suggests the time dependency of the parameters. For another example, we have seen the effect of missing earthquakes in Figure 7, suggesting that parameter c may depend on the magnitude of the earthquake, leading to a significant correlation between c and p . Furthermore, in Section 2.3, it is mentioned that K_0 is correlated with the parameter α . Unstable estimations of K_0 and the α value in the swarm period before the M4.6 earthquake can be seen in Table 2, during which period most of the magnitudes are between 2.5 and 3. This is another reason why the α value is fixed by the corresponding reference parameter α when the nonstationary models are applied. Owing

to the linearly parameterized coefficients of the functions q_μ and q_K in equation (10), the maximizing solutions of the penalized log-likelihood function [equation (16)], in spite of the high dimension, can be obtained uniquely and stably by fixing the three parameters c, α and p .

APPENDIX: SYNTHETIC TEST OF REPRODUCIBILITY OF NONSTATIONARY PATTERNS

We tested our method with synthetic data sets to check if both $\mu(t)$ and $K_0(t)$ can be reproduced by simulated data sets that are similar to observed data sets. We used the reference parameter set (Table 2) with the best estimated $\mu(t)$ and $K_0(t)$ of model 3(a').

The magnitude sequence of the synthetic data was generated on the basis of the Gutenberg–Richter law with a b -value of the original data set ($b = 1.273$). In other words, the magnitude of each earthquake will independently obey an exponential distribution such that $f(M) = \beta \exp\{-\beta(M - M_c)\}$, $M \geq M_c$, where $\beta = b \ln 10$, and $M_c = 2.5$ is the magnitude value above which all earthquakes are detected.

The thinning method [Ogata (1981, 1998)] is adopted for data simulation. A total of 470 events were simulated with a threshold magnitude of 2.5. Model 3(a') was then fitted to the simulated data sets, with a change point at the same time as the original data (between the 182nd and 183rd event). Results are shown in Figure 7; the estimated $\mu(t)$ and $K_0(t)$ appear to be similar to the original $\mu(t)$ and $K_0(t)$ in Figure 6, respectively, within a 2σ error.

Acknowledgments. We are grateful to the Japan Meteorological Agency (JMA), the National Research Institute for Earth Science and Disaster Prevention (NIED) and the universities for the hypocenter data. We used the TSEIS visualization program package [Tsuruoka (1996)] for the study of hypocenter data.

REFERENCES

- ADELFINO, G. and OGATA, Y. (2010). Hybrid kernel estimates of space–time earthquake occurrence rates using the epidemic-type aftershock sequence model. *Ann. Inst. Statist. Math.* **62** 127–143. [MR2577443](#)
- AKAIKE, H. (1973). Information theory and an extension of the maximum likelihood principle. In *Second International Symposium on Information Theory (Tsahkadsor, 1971)* 267–281. Akadémiai Kiadó, Budapest. [MR0483125](#)
- AKAIKE, H. (1974). A new look at the statistical model identification. *IEEE Trans. Automat. Control* **AC-19** 716–723. System identification and time-series analysis. [MR0423716](#)
- AKAIKE, H. (1977). On entropy maximization principle. In *Applications of Statistics* (P. R. KRISHNAIAN, ed.) 27–41. North-Holland, Amsterdam. [MR0501456](#)

- AKAIKE, H. (1980). Likelihood and the Bayes procedure. In *Bayesian Statistics (Valencia, 1979)* (J. M. BERNARDO, M. H. DE GROOT, D. V. LINDLEY and A. F. M. SMITH, eds.) 143–166. Univ. Press, Valencia, Spain. [MR0638876](#)
- AKAIKE, H. (1985). Prediction and entropy. In *A Celebration of Statistics* (A. C. ATKINSON and E. FIENBERG, eds.) 1–24. Springer, New York. [MR0816143](#)
- AKAIKE, H. (1987). Factor analysis and AIC. *Psychometrika* **52** 317–332. [MR0914459](#)
- BALDERAMA, E., PAIK SCHOENBERG, F., MURRAY, E. and RUNDEL, P. W. (2012). Application of branching models in the study of invasive species. *J. Amer. Statist. Assoc.* **107** 467–476. [MR2980058](#)
- BANSAL, A. R. and OGATA, Y. (2013). A non-stationary epidemic type aftershock sequence model for seismicity prior to the December 26, 2004 M9.1 Sumatra-Andaman Islands mega-earthquake. *J. Geophys. Res.* **118** 616–629.
- CHAVEZ-DEMOULINA, V. and MCGILLB, J. A. (2012). High-frequency financial data modeling using Hawkes processes. *J. Bank. Financ.* **36** 3415–3426.
- DALEY, D. and VERE-JONES, D. (2003). *An Introduction to the Theory of Point Processes*, 2nd ed. Springer, New York.
- GOOD, I. J. (1965). *The Estimation of Probabilities. An Essay on Modern Bayesian Methods*. MIT Press, Cambridge, MA. [MR0185724](#)
- GOOD, I. J. and GASKINS, R. A. (1971). Nonparametric roughness penalties for probability densities. *Biometrika* **58** 255–277. [MR0319314](#)
- HAINZL, S. and OGATA, Y. (2005). Detecting fluid signals in seismicity data through statistical earthquake modeling. *J. Geophys. Res.* **110** B5, B05S07.
- HASSAN ZADEH, A. and SHARDA, R. (2012). Modeling brand post popularity in online social networks. Social Science Research Network. Available at SSRN 2182711.
- HAWKES, A. G. (1971). Spectra of some self-exciting and mutually exciting point processes. *Biometrika* **58** 83–90. [MR0278410](#)
- HAWKES, A. G. and ADAMOPOULOS, L. (1973). Cluster models for earthquakes—regional comparisons. *Bull. Int. Stat. Inst.* **45** 454–461.
- HAWKES, A. G. and OAKES, D. (1974). A cluster process representation of a self-exciting process. *J. Appl. Probab.* **11** 493–503. [MR0378093](#)
- HERRERA, R. and SCHIPP, B. (2009). Self-exciting extreme value models for stock market crashes. In *Statistical Inference, Econometric Analysis and Matrix Algebra* 209–231. Physica-Verlag HD, Heidelberg.
- JAPAN METEOROLOGICAL AGENCY (2009). The Iwate-Miyagi Nairiku earthquake in 2008. *Rep. Coord. Comm. Earthq. Predict* **81** 101–131. Available at http://cais.gsi.go.jp/YOCHIREN/report/kaihou81/03_04.pdf.
- JORDAN, T. H., CHEN, Y.-T. and GASPARINI, P. (2012). Operational earthquake forecasting. State of knowledge and guidelines for utilization. *Ann. Geophys.* **54** 315–391.
- KAGAN, Y. Y. and KNOPOFF, L. (1987). Statistical short-term earthquake prediction. *Science* **236** 1563–1567.
- KENDALL, D. G. (1949). Stochastic processes and population growth. *J. Roy. Statist. Soc. Ser. B.* **11** 230–264. [MR0034977](#)
- KUMAZAWA, T., OGATA, Y. and TODA, S. (2010). Precursory seismic anomalies and transient crustal deformation prior to the 2008 $M_w = 6.9$ Iwate-Miyagi Nairiku, Japan, earthquake. *J. Geophys. Res.* **115** B10312.
- LAPLACE, P. S. (1774). Memoir on the probability of causes of events. Mémoires de mathématique et de physique, tome sixième (English translation by S. M. Stigler, 1986). *Statist. Sci.* **1** 364–378.
- LLENOS, A. L., MCGUIRE, J. J. and OGATA, Y. (2009). Modeling seismic swarms triggered by aseismic transients. *Earth Planet. Sci. Lett.* **281** 59–69.

- LOMBARDI, A. M., COCCO, M. and MARZOCCHI, W. (2010). On the increase of background seismicity rate during the 1997–1998 Umbria–Marche, central Italy, sequence: Apparent variation or fluid-driven triggering? *Bull. Seismol. Soc. Amer.* **100** 1138–1152.
- LOMNITZ, C. (1974). *Global Tectonic and Earthquake Risk*. Elsevier, Amsterdam.
- MOHLER, G. O., SHORT, M. B., BRANTINGHAM, P. J., SCHOENBERG, F. P. and TITA, G. E. (2011). Self-exciting point process modeling of crime. *J. Amer. Statist. Assoc.* **106** 100–108. [MR2816705](#)
- OGATA, Y. (1978). The asymptotic behaviour of maximum likelihood estimators for stationary point processes. *Ann. Inst. Statist. Math.* **30** 243–261. [MR0514494](#)
- OGATA, Y. (1981). On Lewis’ simulation method for point processes. *IEEE Trans. Inform. Theory* **27** 23–31.
- OGATA, Y. (1985). Statistical models for earthquake occurrences and residual analysis for point processes. Research Memorandum No. 388 (21 May), The Institute of Statistical Mathematics, Tokyo. Available at <http://www.ism.ac.jp/editsec/resmemo-e.html>.
- OGATA, Y. (1986). Statistical models for earthquake occurrences and residual analysis for point processes. *Mathematical Seismology* **1** 228–281.
- OGATA, Y. (1988). Statistical models for earthquake occurrences and residual analysis for point processes. *J. Amer. Statist. Assoc.* **83** 9–27.
- OGATA, Y. (1989). Statistical model for standard seismicity and detection of anomalies by residual analysis. *Tectonophysics* **169** 159–174.
- OGATA, Y. (1992). Detection of precursory relative quiescence before great earthquakes through a statistical model. *J. Geophys. Res.* **97** 19845–19871.
- OGATA, Y. (1998). Space–time point-process models for earthquake occurrences. *Ann. Inst. Statist. Math.* **50** 379–402.
- OGATA, Y. (1999). Seismicity analysis through point-process modeling: A review. *Pure Appl. Geophys.* **155** 471–507.
- OGATA, Y. (2001). Exploratory analysis of earthquake clusters by likelihood-based trigger models. *J. Appl. Probab.* **38A** 202–212. [MR1915545](#)
- OGATA, Y. (2004). Space–time model for regional seismicity and detection of crustal stress changes. *J. Geophys. Res.* **109** B03308.
- OGATA, Y. (2005). Detection of anomalous seismicity as a stress change sensor. *J. Geophys. Res.* **110** B05S06.
- OGATA, Y. (2006a). Seismicity anomaly scenario prior to the major recurrent earthquakes off the East coast of Miyagi prefecture, northern Japan. *Tectonophysics* **424** 291–306.
- OGATA, Y. (2006b). Fortran programs statistical analysis of seismicity—Updated version, (SASeis2006). *Computer Science Monograph* No. 33, The Institute of Statistical Mathematics, Tokyo, Japan. Available at http://www.ism.ac.jp/editsec/csm/index_j.html.
- OGATA, Y. (2007). Seismicity and geodetic anomalies in a wide preceding the Niigata-Ken-Chuetsu earthquake of 23 October 2004, central Japan. *J. Geophys. Res.* **112** B10301.
- OGATA, Y. (2010). Anomalies of seismic activity and transient crustal deformations preceding the 2005 M7.0 earthquake west of Fukuoka. *Pure Appl. Geophys.* **167** 1115–1127.
- OGATA, Y. (2011a). Long-term probability forecast of the regional seismicity that was induced by the M9 Tohoku-Oki earthquake. *Report of the Coordinating Committee for Earthquake Prediction* **88** 92–99.
- OGATA, Y. (2011b). Significant improvements of the space–time ETAS model for forecasting of accurate baseline seismicity. *Earth Planets Space* **63** 217–229.
- OGATA, Y. (2012). Tohoku earthquake aftershock activity (in Japanese). *Report of the Coordinating Committee for Earthquake Prediction* **88** 100–103.

- OGATA, Y., JONES, L. M. and TODA, S. (2003). When and where the aftershock activity was depressed: Contrasting decay patterns of the proximate large earthquakes in southern California. *J. Geophys. Res.* **108** B6, 2318.
- OGATA, Y. and KATSURA, K. (1993). Analysis of temporal and special heterogeneity of magnitude frequency distribution inferred from earthquake catalogues. *Geophys. J. Int.* **113** 727–738.
- OGATA, Y. and KATSURA, K. (2006). Immediate and updated forecasting of aftershock hazard. *Geophys. Res. Lett.* **33** L10305.
- OGATA, Y., KATSURA, K. and TANEMURA, M. (2003). Modelling heterogeneous space–time occurrences of earthquakes and its residual analysis. *J. Roy. Statist. Soc. Ser. C* **52** 499–509. [MR2012973](#)
- OKUTANI, T. and IDE, S. (2011). Statistic analysis of swarm activities around the Boso Peninsula, Japan: Slow slip events beneath Tokyo Bay? *Earth Planets Space* **63** 419–426.
- OMI, T., OGATA, Y., HIRATA, Y. and AIHARA, K. (2013). Forecasting large aftershocks within one day after the main shock. *Sci. Rep.* **3** 2218.
- PENG, R. D., SCHOENBERG, F. P. and WOODS, J. A. (2005). A space–time conditional intensity model for evaluating a wildfire hazard index. *J. Amer. Statist. Assoc.* **100** 26–35. [MR2166067](#)
- REASENBERG, P. (1985). Second-order moment of central California seismicity, 1969–1982. *J. Geophys. Res.* **90** B7, 5479–5495.
- SCHOENBERG, F. P., PENG, R. and WOODS, J. (2003). On the distribution of wild fire sizes. *Environmetrics* **14** 583–592.
- TERAKAWA, T., HASHIMOTO, C. and MATSU’URA, M. (2013). Changes in seismic activity following the 2011 Tohoku-Oki earthquake: Effects of pore fluid pressure. *Earth Planet. Sci. Lett.* **365** 17–24.
- TERAKAWA, T. and MATSU’UARA, M. (2010). The 3-d tectonic stress fields in and around Japan inverted from centroid moment tensor data of seismic events. *Tectonics* **29** (TC6008).
- TERAKAWA, T., MILLER, S. and DEICHMANN, N. (2012). High fluid pressure and triggered earthquakes in the enhanced geothermal system in Basel, Switzerland. *J. Geophys. Res.* **117** B07305, 15 pp.
- TODA, S., LIAN, L. and ROSS, S. (2011). Using the 2011 M = 9.0 Tohoku earthquake to test the Coulomb stress triggering hypothesis and to calculate faults brought closer to failure. *Earth Planets Space* **63** 725–730.
- TODA, S., STEIN, R. S. and JIAN, L. (2011). Widespread seismicity excitation throughout central Japan following the 2011 M = 9.0 Tohoku earthquake, and its interpretation in terms of Coulomb stress transfer. *Geophys. Res. Lett.* **38** L00G03.
- TSURUOKA, H. (1996). Development of seismicity analysis software on workstation (in Japanese). *Tech. Res. Rep.* **2** 34–42. Earthq. Res. Inst., Univ. of Tokyo, Tokyo.
- UTSU, T. (1961). Statistical study on the occurrence of aftershocks. *Geophys. Mag.* **30** 521–605.
- UTSU, T. (1962). On the nature of three Alaskan aftershock sequences of 1957 and 1958. *Bull. Seismol. Soc. Amer.* **52** 279–297.
- UTSU, T. (1969). Aftershocks and earthquake statistics (I)—Some parameters which characterize an aftershock sequence and their interrelations. *J. Fac. Sci. Hokkaido Univ., Ser. VII* **3** 129–195.
- UTSU, T. (1970). Aftershocks and earthquake statistics (II)—Further investigation of aftershocks and other earthquake sequences based on a new classification of earthquake sequences. *J. Fac. Sci. Hokkaido Univ., Ser. VII* **3** 197–266.

- UTSU, T. (1971). Aftershocks and earthquake statistics (III)—Analyses of the distribution of earthquakes in magnitude, time, and space with special consideration to clustering characteristics of earthquake occurrence (1). *J. Fac. Sci. Hokkaido Univ., Ser. VII* **3** 379–441.
- UTSU, T. (1972). Aftershocks and earthquake statistics (IV)—Analyses of the distribution of earthquakes in magnitude, time, and space with special consideration to clustering characteristics of earthquake occurrence (2). *J. Fac. Sci. Hokkaido Univ., Ser. VII* **4** 1–42.
- UTSU, T., OGATA, Y. and MATSU'URA, R. S. (1995). The centenary of the Omori formula for a decay law of aftershock activity. *J. Seismol. Soc. Japan* **7** 233–240.
- UTSU, T. and SEKI, A. (1955). A relation between the area of after-shock region and the energy of main shock (in Japanese). *Zisin (2)* **7** 233–240.
- VERE-JONES, D. (1970). Stochastic models for earthquake occurrence. *J. Roy. Statist. Soc. Ser. B* **32** 1–62. [MR0272087](#)
- VERE-JONES, D. and DAVIES, R. B. (1966). A statistical study of earthquakes in the main seismic area of New Zealand. Part II: Time series analyses. *N. Z. J. Geol. Geophys.* **9** 251–284.
- ZHUANG, J. and OGATA, Y. (2006). Properties of the probability distribution associated with the largest earthquake in a cluster and their implications to foreshocks. *Phys. Rev. E* **73** 046134.
- ZHUANG, J., OGATA, Y. and VERE-JONES, D. (2002). Stochastic declustering of space–time earthquake occurrences. *J. Amer. Statist. Assoc.* **97** 369–380. [MR1941459](#)
- ZHUANG, J., OGATA, Y. and VERE-JONES, D. (2004). Analyzing earthquake clustering features by using stochastic reconstruction. *J. Geophys. Res.* **109** B5, B05301.

THE INSTITUTE OF STATISTICAL MATHEMATICS
10-3 MIDORI-CHO, TACHIKAWA
TOKYO 190-8562
JAPAN
E-MAIL: tkuma@ism.ac.jp

THE INSTITUTE OF STATISTICAL MATHEMATICS
10-3 MIDORI-CHO, TACHIKAWA
TOKYO 190-8562
JAPAN
AND
EARTHQUAKE RESEARCH INSTITUTE
UNIVERSITY OF TOKYO
1-1-1 YAYOI, BUNKYO-KU
TOKYO 113-0032
JAPAN